Preparation of spherical graphite from Bao Ha natural flake graphite for lithium-ion battery anode applications

Vu Tri Thien*, Nguyen Tran Hung, La Duc Duong

Institute of Materials, Biology and Environment, Academy of Military Science and Technology, 17 Hoang Sam, Nghia Do, Hanoi, Vietnam.
*Corresponding author: Thienkqh140309@gmail.com
Received 13 May 2026; Revised 27 Jul. 2026; Accepted 15 Sep. 2026; Published 15 Oct. 2026.
DOI: https://doi.org/10.54939/1859-1043.j.mst.114.2026.128-134

ABSTRACT

Spherical graphite (SG) was prepared from Bao Ha natural flake graphite (FG) by mechanical milling. The obtained SG exhibited a near-spherical morphology and particle sizes mainly ranging from 10 to 30 µm. EDX, XRD, and Raman analyses showed that carbon was the main component and that the graphitic structure was largely preserved after spheroidization. Electrochemical tests demonstrated improved cycling performance, with SG retaining approximately 250 mAh.g^{-1} after 100 cycles at 100 mA.g^{-1}, compared with 150 mAh.g^{-1} for FG. These results indicate that mechanical spheroidization improves the lithium-storage performance of Bao Ha natural graphite under the investigated conditions.

Keywords: Flake graphite; Spherical graphite; Lithium-ion batteries; Anodes.

1. INTRODUCTION

Lithium-ion batteries (LIBs) are widely used in portable electronics, electric vehicles, and stationary energy-storage systems owing to their high energy density, energy efficiency, and long cycle life [1, 2]. Although alloy-type and conversion-type anodes offer higher theoretical capacities than graphite, their practical applications remain limited by large volume changes, low electrical conductivity, unstable solid electrolyte interphase formation, low initial Coulombic efficiency, and insufficient cycling stability [3-5]. Carbon-based materials, particularly graphite, therefore remain the predominant commercial anodes because of their structural stability, reversible Li^+ intercalation/deintercalation, low operating potential, high electrical conductivity, natural abundance, and cost-effectiveness. Graphite has a theoretical capacity of 372 mAh.g^{-1} and is reportedly used in more than 90% of commercial LIBs. Nevertheless, its electrochemical performance is strongly influenced by particle morphology, size distribution, surface properties, and structural characteristics [6].

In the early stage of LIB commercialization, natural flake graphite (FG) was widely used as the anode material. However, FG suffers from several drawbacks, including limited rate capability, rapid capacity fading, low tap density, and difficulties in achieving homogeneous electrode packing. To overcome these limitations, spheroidization technology has been developed to transform FG into spherical graphite (SG), representing a significant milestone in the commercialization of high-performance graphite anodes. Compared with conventional FG, SG exhibits higher tap density and volumetric energy density, improved electrical conductivity and lithium-ion diffusion kinetics, as well as reduced side reactions with the electrolyte. Previous studies have demonstrated that achieving high-quality SG requires careful control of the properties of the raw FG, together with optimization of the milling and air classification processes [7, 8].

Vietnam possesses approximately 29.3 million tons of graphite resources, nearly 70% of which are located in Lao Cai Province. The Bao Ha deposit contains about 3.2 million tons of explored reserves, predominantly flake graphite (90–95%) [9]. Its abundant coarse flakes make Bao Ha graphite a promising precursor for spherical graphite production. This study investigates the preparation of SG from Bao Ha natural FG by mechanical milling and compares the morphology, structure, composition, and electrochemical performance of FG and SG.

2. EXPERIMENTAL

2.1. Materials and equipment

Natural flake graphite obtained from the Bao Ha graphite mine (Lao Cai, Vietnam) with particle sizes ranging from 10 to 50 μm and a carbon content of 90 - 94 wt.% was used as the starting material. The spheroidization process was carried out using a spheroidization mill (LEAP, China).

2.2. Preparation of spherical graphite

FG with a particle-size range of 10 – 50 μm was spheroidized under dry conditions at a milling-disc speed of 1800 rpm for 40 min. The grinding and classification airflow rates were 800 and 200 $m^3.h^{-1}$, respectively. The spheroidization yield was calculated based on the mass ratio between the obtained SG collected by the cyclone separator and the initial FG feed according to the following equation:

$$H = \frac{m_2}{m_1} \times 100\% \quad (1)$$

where H is the spheroidization yield (%), m_1 is the mass of the initial flake graphite (kg), and m_2 is the mass of the spherical graphite collected after spheroidization (kg).

2.3. Material characterization

The morphology and elemental composition of the samples were characterized using scanning electron microscopy coupled with energy-dispersive X-ray spectroscopy (SEM-EDX, Hitachi S-4800). The particle size distribution of the SG samples was measured using a Horiba Partica LA-950V2 laser diffraction particle size analyzer. The crystalline structure of the materials was investigated by X-ray diffraction (XRD, Bruker D8 Advance). The structural characteristics and degree of graphitization of the carbon materials were further analyzed by Raman spectroscopy using a Thermo Scientific DXR3 Raman microscope.

2.4. Electrochemical measurements

The working electrodes were prepared by mixing graphite powder as the active material with polyvinylidene fluoride (PVDF) binder and Super P conductive carbon at a weight ratio of 8:1:1 using a ball-milling process for 45 min. The resulting slurry was coated onto carbon-coated copper foil serving as the current collector and subsequently dried under vacuum at 80 ^oC for 24 h. CR2032 coin-type half cells were assembled using the prepared electrode as the working electrode and lithium metal foil as both the counter and reference electrodes. A polypropylene separator (Celgard, 19 mm in diameter and 25 μm in thickness) and 1 M $LiPF_6$ dissolved in a mixed solvent of ethylene carbonate (EC), dimethyl carbonate (DMC), and diethyl carbonate (DEC) were employed as the separator and electrolyte, respectively. The electrochemical performance of the samples was evaluated using a WonATech WBCS 3000L32 battery testing system. Cyclic voltammetry (CV) measurements were conducted within a voltage range of 0.01-2.0 V at a scan rate of 0.1 $mV.s^{-1}$. Galvanostatic charge-discharge (GCD) tests were performed in the voltage range of 0.01-2.0 V at a current density of 100 $mA.g^{-1}$.

3. RESULTS AND DISCUSSION

3.1. Characterization of the natural flake graphite precursor

The morphology of the natural flake graphite (FG) was investigated by scanning electron microscopy as shown in Figure 1. The FG sample exhibits a typical layered structure consisting of graphite flakes with lateral sizes ranging from 10 to approximately 50 μm and thicknesses of about 2.5 - 4.0 μm. The graphite flakes possess relatively flat surfaces, sharp edges, and stacked layered features, which are characteristic of natural flake graphite. From a morphological viewpoint, this flake-like structure is favorable for the mechanical spheroidization process. Under the combined

effects of impact, friction, and air classification inside the milling system, the graphite flakes can be fractured, exfoliated, edge-abraded, bent, and rearranged into nearly spherical particles. Therefore, the observed morphology of the Bao Ha FG precursor indicates its suitability for producing spherical graphite through mechanical milling.

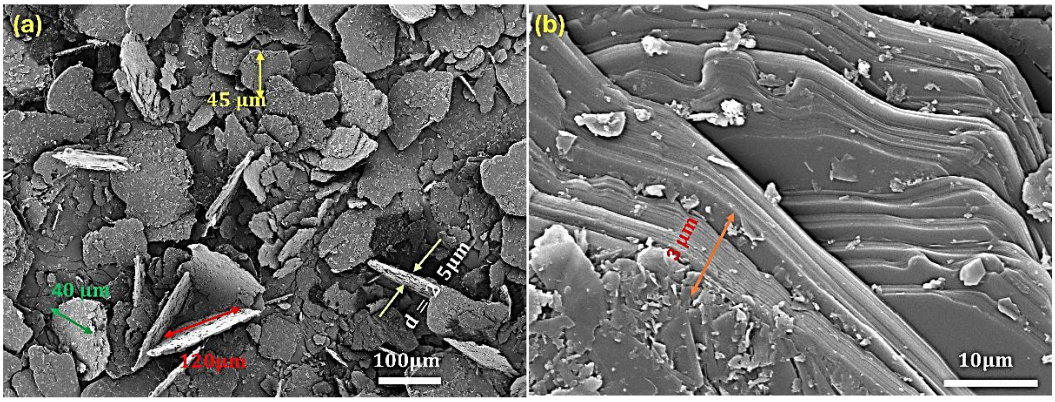

Figure 1. *SEM images of FG at (a) low and (b) high magnifications.*

Besides the morphological characteristics, the crystal structure of FG was further examined by XRD and Raman spectroscopy (Figure 2). As shown in Figure 2a, four prominent diffraction peaks located at 2θ = 26.51°, 42.40 °, 44.50 °, and 54.71 ° are assigned to (002), (100), (101), and (004) planes of graphite, respectively, which are consistent with the standard graphite pattern (JCPDS No. 41-1487). The sharp and intense (002) reflection suggests that the FG sample possesses a highly crystalline and well-ordered graphitic layered structure [11].

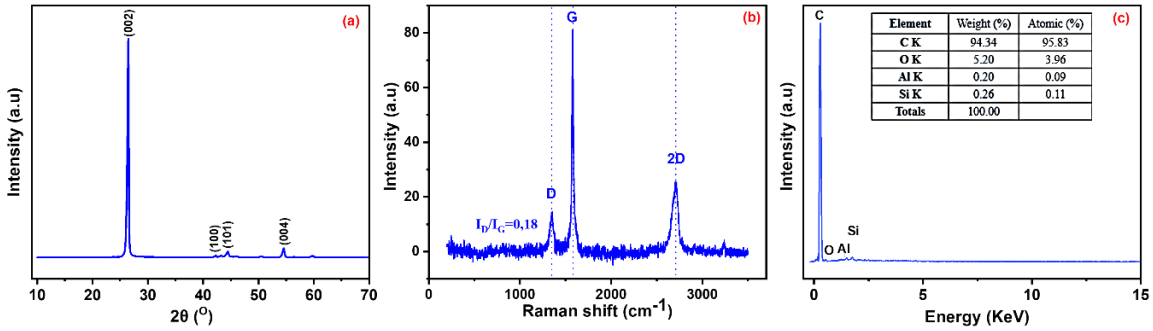

Figure 2. *X-ray diffraction pattern (a), Raman spectrum (b), EDX spectrum (c) of the natural flake graphite.*

The Raman spectrum further confirms the structural characteristics of the FG sample through the presence of the characteristic D, G, and 2D bands (Figure 2b). The intensity ratio of the D and G bands (I_D/I_G) is widely used to evaluate the defect density and structural ordering of graphitic carbon materials. The D band located at approximately 1350 cm^{-1} is associated with structural defects, grain boundaries, and the disruption of the translational symmetry of the graphite lattice, whereas the G band centered at around 1580 cm^{-1} corresponds to the in-plane vibration of ordered sp^2 bonded carbon atoms. A lower I_D/I_G ratio generally indicates a higher degree of crystallinity and a lower defect density [12]. In the present study, the calculated I_D/I_G ratio was 0.18, indicating that the FG sample possesses a highly ordered graphitic structure with a high degree of graphitization. Moreover, the distinct appearance of the 2D band further demonstrates the well-developed layered structure and the relatively good stacking order of the graphene layers. The high crystallinity of FG is also beneficial for electronic conductivity and facilitates the reversible intercalation/deintercalation of Li^+ ions when used as an anode material for lithium-ion batteries.

The chemical composition of the FG sample was examined by EDX analysis, as shown in Figure 2c. The results indicate that carbon is the predominant element, accounting for 94.34 wt.% and 95.83 at.%. In addition to carbon, small amounts of oxygen, aluminum, and silicon were detected, with contents of 5.20, 0.20, and 0.26 wt.%, respectively. The high carbon content suggests that the Bao Ha natural flake graphite is of suitable quality for further processing and spheroidization.

3.2. Characterization of the prepared spherical graphite

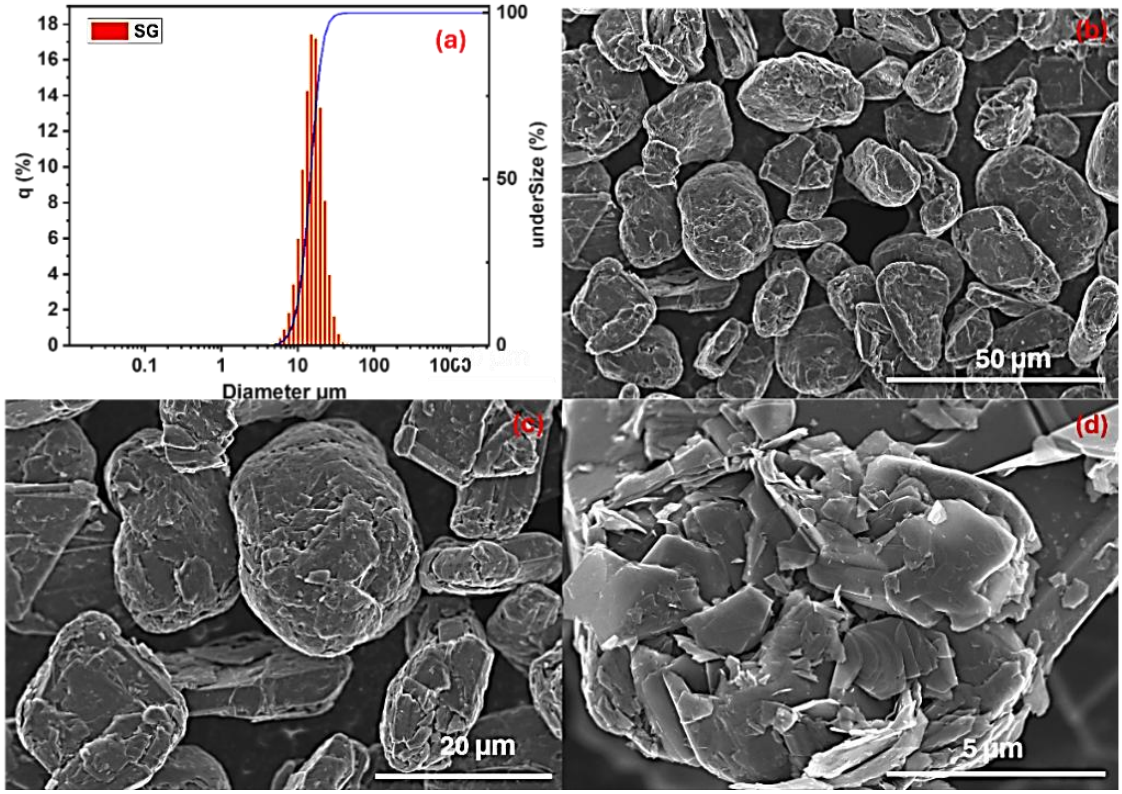

Figure 3. *Particle size distribution (a) and SEM micrographs at different magnifications (b–d) of the spherical graphite obtained by mechanical spheroidization.*

Figure 3 shows the particle size distribution and SEM images of the prepared SG. As presented in Figure 3a, the SG particles are mainly distributed in the range of 10 - 30 µm. This result is consistent with the SEM observations in Figures 3b-d, which clearly reveal a significant morphological transformation after the spheroidization process. Compared with the initial flake graphite precursor, the large, flat graphite flakes were converted into nearly spherical or ellipsoidal particles. However, stacked graphite layers and partially rounded edges can still be observed on the surface of some particles, suggesting that the spheroidization process occurs through flake fragmentation, bending, folding, layer rearrangement, and edge abrasion under mechanical forces. This morphological evolution confirms the suitability of Bao Ha natural flake graphite as a precursor for the preparation of spherical graphite. The structural characteristics of the prepared SG sample are shown in Figure 4. The XRD pattern of SG (Figure 4a) retains the characteristic diffraction peaks of graphite, particularly the intense (002) reflection. This indicates that the mechanical spheroidization process mainly modifies the particle morphology and size, while the graphitic crystal structure is largely preserved. This result is important because the retention of the layered graphite structure is essential for the reversible intercalation/deintercalation of Li^+ ions in anode materials. The Raman spectrum of SG (Figure 4b) also exhibits the typical D, G, and 2D bands of graphitic carbon. Compared with the initial FG sample, the slightly increased I_D/I_G ratio

of SG, from 0.18 to 0.20, suggests a minor increase in structural defects, edge sites, and active surface sites generated during mechanical milling. However, this change is insignificant and does not alter the graphitic nature of the material. These results confirm that the spheroidization process effectively transforms the particle morphology while maintaining the intrinsic graphitic structure of the natural graphite precursor.

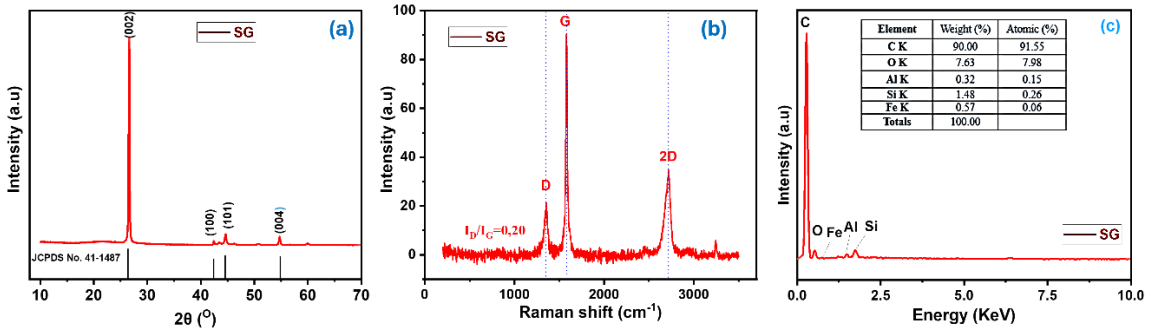

Figure 4. (a) XRD pattern, (b) Raman spectrum, and (c) EDX spectrum of SG.

The EDX spectrum of the prepared SG sample (Figure 4c) shows that carbon remains the predominant element, with a content of approximately 90 wt.%. The weak signals of impurity elements, such as Si, Al, and Fe, indicate that a small number of mineral impurities remain in the material after spheroidization. Compared with the elemental composition of the initial FG sample, the appearance of Fe in SG may be attributed to mechanical abrasion from the milling equipment during the spheroidization process, resulting in the adhesion of Fe-containing species on the particle surface. The variation in carbon content between FG and SG is mainly associated with the change in oxygen-containing impurities during mechanical processing, which may exist in the form of metal or mineral oxides such as Fe_2O_3, Al_2O_3, and SiO_2.

3.3. Electrochemical characterization

The electrochemical properties of the materials are presented in Figure 5. Figure 5(a) shows the cyclic voltammetry (CV) curves of FG. During the first cathodic scan, in addition to the main reduction peak at approximately 0.15 V, which is associated with Li^+ intercalation into the graphite layers to form the LiC_6 phase, two additional reduction peaks are observed at around 0.7 V and 1.4 V. The peak at approximately 0.7 V can be assigned to electrolyte decomposition and the formation of the solid electrolyte interphase (SEI) layer on the graphite surface during the initial cycle. Meanwhile, the reduction peak at around 1.4 V may be related to the reduction of oxygen-containing functional groups, residual mineral impurities, or highly active surface sites of natural graphite. These additional reduction peaks significantly decrease or nearly disappear in the subsequent cycles, indicating that they correspond to irreversible reactions mainly occurring during the initial activation process. The oxidation peak located at approximately 0.25 - 0.30 V is attributed to Li^+ deintercalation from the graphitic structure [13]. Figure 5(b) presents the CV curves of spherical graphite (SG). Like FG, SG exhibits the characteristic redox peaks of graphite, including a cathodic peak at approximately 0.15 V and an anodic peak at around 0.25 - 0.30 V, corresponding to the reversible intercalation/deintercalation of Li^+ ions. In the first cathodic scan, a weak reduction signal at approximately 0.7 V can still be observed, indicating that SEI formation also occurs on the SG surface, although the extent of side reactions is reduced compared with FG. Notably, the additional reduction peak at around 1.4 V is almost absent in the SG electrode. This difference suggests that the spheroidization process effectively reduces highly active edge planes, structural defects, and reactive surface sites, thereby suppressing the reduction of oxygen-containing groups, surface impurities, and electrolyte-related side reactions at higher potentials.

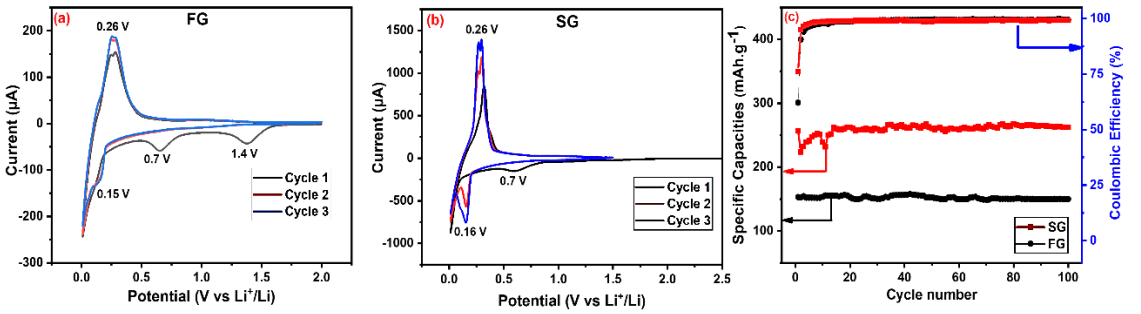

Figure 5. *CV curves of (a) FG and (b) SG, and (c) their cycling performance and Coulombic efficiency at 100 mA g^{-1}.*

Figure 5(c) shows the cycling performance and Coulombic efficiency of FG and SG at a current density of 100 mA.g^{-1}. SG exhibits a higher and more stable specific capacity than FG over 100 cycles. After 100 cycles, SG maintains a capacity of approximately 250 mAh.g^{-1}, whereas FG delivers only about 150 mAh.g^{-1}. The initial Coulombic efficiency of SG is also higher than that of FG, consistent with the CV results, indicating fewer irreversible side reactions during the first cycle. After the initial cycles, the Coulombic efficiency rapidly approaches nearly 100%, demonstrating the formation of a stable SEI layer and highly reversible Li^+ intercalation/deintercalation. These results confirm that spheroidization improves Li^+ diffusion kinetics, enhances lithium-storage capacity, and suppresses surface side reactions in natural graphite [14]. For a clearer comparison of the physicochemical and electrochemical characteristics of the two materials, the key parameters of FG and SG are summarized in Table 1.

Table 1. *Comparison of the physicochemical and electrochemical characteristics of FG and SG.*

Parameter	FG	SG
Particle-size range	10-50 μm	10-30 μm
Carbon content	94.34 wt.%	90 wt.%
I_D/I_G	0.18	0.20
Capacity after 100 cycles	150 mAh.g^{-1}	250 mAh.g^{-1}
Initial Coulombic efficiency	65%	78%

4. CONCLUSIONS

In this study, spherical graphite was successfully prepared from Bao Ha natural flake graphite, Lao Cai, Vietnam, by a mechanical milling process. The obtained SG exhibited a relatively uniform near-spherical morphology, with particle sizes mainly distributed in the range of 10-30 μm, while retaining the characteristic graphitic crystal structure of the original graphite. Under the present half-cell test conditions, SG retained approximately 250 mAh.g^{-1} after 100 cycles at 100 mA.g^{-1}, compared with approximately 150 mAh.g^{-1} for FG. These results demonstrate that spheroidization improves the lithium-storage behavior of the investigated material. However, further optimization and purification, together with evaluation of yield, tap density, metallic impurities, repeatability, initial Coulombic efficiency, and rate performance, are required before practical battery-grade applicability can be established.

REFERENCES

[1]. Yoshino, "*The lithium-ion battery: Two breakthroughs in development and two reasons for the Nobel Prize*", Bulletin of the Chemical Society of Japan, Vol. 95, No. 1, pp. 195–197, (2022). DOI: 10.1246/bcsj.20210338.

[2]. P. U. Nzereogu, A. D. Omah, F. I. Ezema, E. I. Iwuoha and A. C. Nwanya, "*Anode materials for lithium-ion batteries: A review*", Applied Surface Science Advances, Vol. 9, p. 100233, (2022). DOI:

10.1016/j.apsadv.2022.100233.
[3]. K. T. Pham et al., "*Comparative study on architecture-dependent electrochemical properties of aluminum anode materials for lithium-ion batteries*", ChemistrySelect, Vol. 9, No. 43, p. e202404889, (2024). DOI: 10.1002/slct.202404889.
[4]. K. T. Pham et al., "*Enhancing electrochemical properties for aluminum-based anode materials for LIBs with PVP-derived carbon protective coating*", J. Mil. Sci. Technol., No. IMBE, pp. 214–220, (2025). DOI: 10.54939/1859-1043.j.mst.IMBE.2025.214-220.
[5]. T. T. Vu et al., "*Scalable synthesis of spherical graphite/ZnO composite anodes for high-performance lithium-ion batteries*", RSC Advances, Vol. 16, No. 3, pp. 2754–2766, (2026). DOI: 10.1039/D5RA09552B.
[6]. L. Zhao et al., "*Revisiting the roles of natural graphite in ongoing lithium-ion batteries*", Advanced Materials, Vol. 34, No. 18, p. 2106704, (2022). DOI: 10.1002/adma.202106704.
[7]. J. Zou et al., "*Spheroidization mechanism of flake graphite in cascaded air classifier mill process*", Carbon, Vol. 247, p. 121070, (2026). DOI: 10.1016/j.carbon.2025.121070.
[8]. Z. Tang, X. Zhang, D. Huang, B. Wang and J. Wang, "*Critical thickness and its role in the spheroidization of natural flake graphite*", Carbon Neutralization, Vol. 5, No. 1, p. e70079, (2026). DOI: 10.1002/cnl2.70079.
[9]. H. T. Tran, A. D. Dao and A. N. Tran, "*Nghiên cứu công nghệ tuyển quặng graphit mỏ Bảo Hà, tỉnh Lào Cai*", Vol. XXXI, No. 4, pp. 60–63, (2017). (in Vietnamese)
[10]. S. Fischer, S. Doose, J. Müller, C. Höfels and A. Kwade, "*Impact of spheroidization of natural graphite on fast-charging capability of anodes for LIB*", Batteries, Vol. 9, No. 6, p. 305, (2023). DOI: 10.3390/batteries9060305.
[11]. M. Salvatore, G. Carotenuto, S. De Nicola, C. Camerlingo, V. Ambrogi and C. Carfagna, "*Synthesis and characterization of highly intercalated graphite bisulfate*", Nanoscale Research Letters, Vol. 12, No. 1, p. 167, (2017). DOI: 10.1186/s11671-017-1930-2.
[12]. D. Bogachuk et al., "*Comparison of highly conductive natural and synthetic graphites for electrodes in perovskite solar cells*", Carbon, Vol. 178, pp. 10–18, (2021). DOI: 10.1016/j.carbon.2021.01.022.
[13]. J. Xu, X. Wang, N. Yuan, B. Hu, J. Ding and S. Ge, "*Graphite-based lithium-ion battery with ultrafast charging and discharging and excellent low temperature performance*", Journal of Power Sources, Vol. 430, pp. 74–79, (2019). DOI: 10.1016/j.jpowsour.2019.05.024.
[14]. M. Yoshio, H. Wang, K. Fukuda, T. Umeno, T. Abe and Z. Ogumi, "*Improvement of natural graphite as a lithium-ion battery anode material, from raw flake to carbon-coated sphere*", Journal of Materials Chemistry, Vol. 14, No. 11, p. 1754, (2004). DOI: 10.1039/b316702j.

TÓM TẮT

Chế tạo graphite cầu từ graphite vảy tự nhiên Bảo Hà ứng dụng làm vật liệu điện cực âm cho ắc quy lithium-ion

Trong nghiên cứu này, Graphite cầu (SG) được chế tạo từ graphite vảy tự nhiên (FG) mỏ Bảo Hà, Lào Cai bằng phương pháp nghiền cơ học. SG thu được có hình thái gần cầu, với kích thước hạt tập trung chủ yếu trong khoảng 10–30 μm, đồng thời vẫn duy trì cấu trúc graphitic đặc trưng của graphite tự nhiên. Tại mật độ dòng 100 mA.g^{-1}, SG duy trì dung lượng riêng khoảng 250 mAh.g^{-1} sau 100 chu kỳ, cao hơn đáng kể so với FG khoảng 150 mAh.g^{-1}. Kết quả cho thấy quá trình cầu hóa cơ học cải thiện hiệu năng điện hóa của graphite tự nhiên Bảo Hà trong điều kiện khảo sát, cho thấy tiềm năng phát triển vật liệu này làm anode cho pin lithium-ion.

Từ khóa: Graphite vảy; Graphite cầu; Nghiền tạo cầu; Pin Li-ion; Anode.